Exchange Rates at the Lipid–Protein Interface of Myelin Proteolipid Protein Studied by Spin-Label Electron Spin Resonance

László I. Horváth,[‡] Peter J. Brophy,[§] and Derek Marsh*

Abteilung Spektroskopie, Max-Planck-Institut für biophysikalische Chemie, D-3400 Göttingen, Federal Republic of Germany

Received February 13, 1987; Revised Manuscript Received August 10, 1987

ABSTRACT: The electron spin resonance (ESR) spectra from spin-labeled phospholipids in recombinants of myelin proteolipid apoprotein with dimyristoylphosphatidylcholine have been simulated with the exchanged-coupled Bloch equations to obtain values for both the fraction of motionally restricted lipids and the exchange rate between the fluid and motionally restricted lipid populations. The rate of exchange between the two spin-labeled lipid components is found to lie in the slow exchange regime of nitroxide ESR spectroscopy. The values obtained for the fraction of motionally restricted component in the exchanged-coupled spectra are found to be in good agreement with those obtained previously by spectral subtraction for the same system [Brophy, P. J., Horváth, L. I., & Marsh, D. (1984) *Biochemistry 23*, 860–865]. The rate of lipid exchange off the protein is independent of lipid/protein ratio for a given spin-labeled phospholipid, as expected, and decreases with increasing selectivity of the various phospholipids for the protein. At 30 °C and for ionic strength 0.1 and pH 7.4, the off-rate constants are 4.6×10^6 s^{-1} for phosphatidic acid, 1.1×10^7 s^{-1} for phosphatidylserine, 1.6×10^7 s^{-1} for phosphatidylcholine, and 2.2×10^7 s^{-1} for phosphatidylethanolamine. These values are in the inverse ratio of the relative association constants of the various lipids for the protein (Brophy et al., 1984) and are appreciably slower than the rate of lipid lateral diffusion in dimyristoylphosphatidylcholine bilayers. The exchange rate increases with increasing temperature, with an activation energy of 24 kJ·mol^{-1} for spin-labeled phosphatidic acid in the fluid phase and with a steeper rate of increase in the phase transition region. These results strongly support the ESR spectral subtraction methods used previously to analyze the thermodynamics of lipid–protein interactions.

An important feature of lipid/protein dynamics in biological membranes is the exchange of the lipid molecules at the surface of the intramembranous proteins. This exchange is responsible, at least in part, for interfacing the rigid backbone of the protein to its fluid lipid bilayer environment. In addition, specific interactions between lipid and protein will be reflected in the rate of exchange; in the extreme a highly specific interaction would give rise to very long residence times of the lipid on the surface of the protein.

NMR[1] studies (Seelig et al., 1982; Kang et al., 1979) on various lipid–protein systems have revealed a single-component spectrum from the lipids, indicating that exchange on and off the protein surface is fast on the ^{31}P and ^{2}H NMR time scales ($\lesssim 10^{-3}$ and 10^{-5} s, respectively). ESR spectra of spin-labeled lipids on the other hand have long been known to give rise to two-component spectra in lipid/protein systems (Jost et al., 1973; Marsh & Watts, 1982), suggesting that the exchange is slow on the ESR time scale ($\gtrsim 10^{-8}$ s). Simulations of ESR spectra for spin-labeled chains covalently linked to rhodopsin have demonstrated that the free end of the chain exchanges on and off the protein surface with a lifetime of 10^{-7} s (Davoust & Devaux, 1982). ESR measurements of the collision rate of spin-labeled lipids with the surface of rhodopsin have revealed, as expected, that this is essentially a diffusion-controlled process (Davoust et al., 1983).

Clearly from the point of view of lipid–protein interactions, the lifetime of the lipid molecules on the surface of the protein is the relevant parameter. In the present work we have attempted to measure this parameter for the reconstituted system myelin proteolipid–dimyristoylphosphatidylcholine, which was studied previously by us (Brophy et al., 1984). The method used is the simulation of the two-component ESR spectra from freely diffusible spin-labeled lipids, allowing for exchange between the fluid and motionally restricted lipid populations. The treatment is similar to that previously employed by Davoust and Devaux (1982) for labels covalently linked to the protein. It is found possible to give a consistent description of the dependence of the rates of exchange on lipid/protein ratio, lipid specificity, and temperature.

Materials and Methods

Experimental. Dimyristoylphosphatidylcholine (DMPC) was obtained from Fluka (Buchs, Switzerland). Stearic acid (14-SASL) and phospholipids labeled on the 14-C atom of the *sn*-2 chain (14-PCSL, 14-PESL, 14-PSSL, and 14-PASL) were synthesized as described in Marsh and Watts (1982). Proteolipid protein was extracted from bovine spinal cord myelin and delipidated by gel filtration on Sephadex LH-20 (Pharmacia, Sweden), essentially as described by Brophy (1977). SDS–polyacrylamide gel electrophoresis (Laemmli, 1970) of the delipidated protein revealed bands corresponding to the myelin proteolipid protein (23.5 kDa) and the closely related 20-kDa DM-20 protein, in the ratio of approximately 2–2.5:1. No evidence was found for the presence of the 12-kDa

[‡] Permanent address: Institute of Biophysics, Biological Research Centre, Szeged, Hungary.

[§] Permanent address: Department of Biological Science, Stirling University, Stirling FK9 4LA, U.K.

[1] Abbreviations: ESR, electron spin resonance; Hepes, *N*-(2-hydroxyethyl)piperazine-*N*′-2-ethanesulfonic acid; PLP, myelin proteolipid apoprotein; DMPC, 1,2-dimyristoyl-*sn*-glycero-3-phosphocholine; 14-PCSL, -PESL, -PSSL, and -PASL, 1-acyl-2-[14-(4,4-dimethyloxazolidine-*N*-oxyl)stearoyl]-*sn*-glycero-3-phosphocholine, -phosphoethanolamine, -phosphoserine, and -phosphatidic acid; NMR, nuclear magnetic resonance; SDS, sodium dodecyl sulfate; EDTA, ethylenediaminetetraacetic acid.

0006-2960/88/0427-0046$01.50/0

P-12 protein in the gels of the delipidated preparation. Protein–lipid complexes were reconstituted by dialysis from 2-chloroethanol as described in Brophy et al. (1984). Lipid phosphorus was determined according to Eibl and Lands (1969) and protein according to Lowry et al. (1951). Lipid/protein ratios were calculated by assuming a monomer protein M_r of 25 000. Lipid/protein samples were labeled at a level of 1–2 mol % with a small volume of concentrated spin-label solution in ethanol and subsequent washing. The buffer used was 0.1 M KCl, 1 mM EDTA, and 2 mM Hepes, pH 7.4.

ESR spectra were recorded on a Varian Century Line 9-GHz spectrometer, with nitrogen gas flow temperature regulation. Samples were contained in 1-mm i.d. glass capillaries. Spectral subtractions were performed as described in Marsh (1982). Further details of the experimental methods are given in Brophy et al. (1984).

Simulations of Two-Component Spectra with Exchange. The two-site model for chemical exchange is used in conjunction with the Bloch equations (McConnell, 1958). The rate equations for the spin magnetization associated with the motionally restricted and fluid components, M_b and M_f, respectively, are given by

$$dM_b/dt = -\tau_b^{-1}M_b + \tau_f^{-1}M_f \quad (1)$$

$$dM_f/dt = \tau_b^{-1}M_b - \tau_f^{-1}M_f \quad (2)$$

where τ_b^{-1} and τ_f^{-1} are the probabilities per unit time of transfer from the motionally restricted to the fluid component and vice versa, respectively. These equations assume rapid mixing of the lipids in the fluid pool by lateral diffusion, such that all fluid lipids sample the lipid–protein interface within the lifetime of the motionally restricted lipids, τ_b. At exchange equilibrium, $dM_b/dt = dM_f/dt = 0$, and hence from eq 1 and 2

$$\tau_b^{-1}/\tau_f^{-1} = M_f/M_b = (1-f)/f \quad (3)$$

where f is the fraction of motionally restricted lipid.

The Bloch equations for the response of the spin system to a microwave magnetic field H_1 of angular frequency ω can be written in terms of complex magnetizations, $\hat{M}_b = u_b + iv_b$ and $\hat{M}_f = u_f + iv_f$. Incorporation of the rate equations (eq 1 and 2) yields the following expressions involving the steady-state (complex) magnetizations:

$$[T_{2,b}^{-1} + \tau_b^{-1} - i(\omega - \omega_b)]\hat{M}_b - \tau_f^{-1}\hat{M}_f = i\gamma H_1 M_0 f$$

$$[T_{2,f}^{-1} + \tau_f^{-1} - i(\omega - \omega_f)]\hat{M}_f - \tau_b^{-1}\hat{M}_b = i\gamma H_1 M_0 (1-f) \quad (4)$$

where $T_{2,b}$ and $T_{2,f}$ and ω_b and ω_f are the transverse relaxation times and angular resonance frequencies of the motionally restricted and fluid components, respectively; M_0 is the total magnetization, and γ is the magnetogyric ratio. The total magnetization is thus given by

$$\hat{M} = \hat{M}_b + \hat{M}_f = -\gamma H_1 M_0\{[(\omega - \omega_f) + iT_{2,f}^{-1}]f + [(\omega - \omega_b) + iT_{2,b}^{-1}](1-f) + i(\tau_b^{-1} + \tau_f^{-1})\}/\{[(\omega - \omega_b) + i(T_{2,b}^{-1} + \tau_b^{-1})][(\omega - \omega_f) + i(T_{2,f}^{-1} + \tau_f^{-1})] + \tau_b^{-1}\tau_f^{-1}\} \quad (5)$$

where the imaginary part, $v = v_b + v_f$, gives the intensity of the resonance absorption.

To simulate the entire line shape, a summation must be made over all angular orientations θ of the spin-label director axes relative to the magnetic field direction (Davoust & Devaux, 1982). If it is assumed that the angular orientation is preserved during the exchange between the two environments (model I), the spectra corresponding to transitions between sites with resonance frequencies $\omega_b(\theta)$ and $\omega_f(\theta)$ are added with a weighting factor $p(\theta)\,d\theta = \sin\theta\,d\theta$. Since the nuclear spin orientation is preserved during the exchange, the line shapes corresponding to the $m_I = +1$, 0, and -1 nuclear manifolds are calculated separately. The results of such simulations calculated according to eq 5 with a 5° mesh in θ are given in Figure 1 for various values of the exchange frequency. The relative intensities of the two components are equal, and the spectral parameters are chosen to correspond to typical experimental spectra (see below). Initially, as the exchange frequency is increased, the lines of the two spectral components first broaden, while remaining at their original positions in the absence of exchange (Figure 1a,b). This corresponds to the slow-exchange limit $[\tau_b^{-1}, \tau_f^{-1} \ll (\omega_b - \omega_f)]$. Then, as the rate of exchange increases further, the lines come together (Figure 1d) and finally merge to yield a sharp spectrum whose anisotropy is the mean of that of the two exchanging components (Figure 1f). The latter corresponds to the fast-exchange limit $[\tau_b^{-1}, \tau_f^{-1} \gg (\omega_b - \omega_f)]$. It will be seen below that the experimental spectra from myelin proteolipid–DMPC recombinants correspond to those of the slow-exchange regime for the two spin-label components. This is also the case for many other lipid–protein systems investigated, as evidenced by their essential two-component nature [see, e.g., Marsh (1985)].

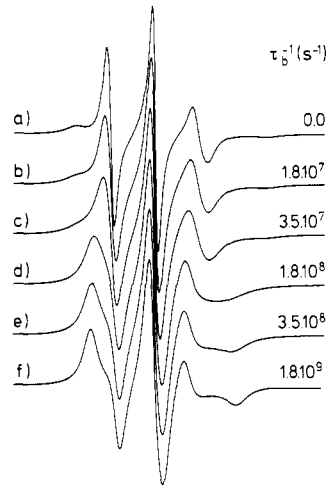

FIGURE 1: Effect of bulk-to-boundary lipid exchange on the spectral line shapes of two-component ESR spectra. Spectral parameters of the two components are given in the supplementary material. The spectral intensity of the two components is in the ratio 1:1. The exchange rate, τ_b^{-1} ($=\tau_f^{-1}$), is varied from 0 to 1.8×10^9 s^{-1} as indicated. Model I is used in the simulations; i.e., the orientation of the spin probes is preserved during the exchange.

An alternative model for the exchange is to assume that spin-labels with a unique director orientation in the fluid component are able to exchange with labels having all possible orientations in the motionally restricted component. This is model II of Davoust and Devaux (1982) and corresponds to the situation in which there is random reorientation of the chain segments on collision with the invaginated protein surface. This model, and also others which involve a spread of director orientations in the fluid component, yields very similar spectra to those for model I in the slow-motion regime, which is that applicable to the present experimental spectra (Davoust & Devaux, 1982; East et al., 1985). Because of the considerable savings in the time required for simulation, model I is therefore used for all subsequent simulations.

In the slow-exchange regime $[\tau_b^{-1}, \tau_f^{-1} \ll (\omega_b - \omega_f)]$, the out-of-phase component of the magnetization in eq 5, which corresponds to the resonance absorption, is given by

$$v(\omega) = \frac{f(T_{2,b}^{-1} + \tau_b^{-1})}{(T_{2,b}^{-1} + \tau_b^{-1})^2 + (\omega_b - \omega)^2} + \frac{(1-f)(T_{2,f}^{-1} + \tau_f^{-1})}{(T_{2,f}^{-1} + \tau_f^{-1})^2 + (\omega_f - \omega)^2} \quad (6)$$

Clearly, in this regime the slow-exchange line shape is a weighted sum of two Lorentzians whose line widths are increased due to lifetime broadening. The amount of the increase in line width is given by the reciprocal of the exchange lifetime, i.e.

$$T_2^{-1} = T_{2,f}^{-1} + \tau_f^{-1} \quad (7)$$

and a similar expression for the motionally restricted component. Equation 6 indicates why the simulations in the slow-exchange regime are relatively insensitive to the model used for the exchange. The lifetime broadening is principally seen in the fluid component, since this has the narrowest lines, and is not dependent on the positions of the lines with which it is exchanging, provided that these are sufficiently far removed to fulfill the slow-exchange condition. This is a quite general feature of slow exchange.

The validity of eq 7 for slow-exchange simulations is tested in Figure 2. The spectral parameters used in the simulations are those appropriate to the experimental spectra of the PLP/DMPC recombinants (see Table I and supplementary material, given later). Because the anisotropy in the fluid component is very low, the line shapes of the individual hyperfine lines correspond quite closely to those of single, first-derivative ESR lines. This is especially true for the low-field line, but even in this case there is still the problem of allowing for the underlying inhomogeneous broadening of the lines. If the inhomogeneous broadening is represented by a Gaussian distribution of Lorentzian lines, Dobryakov and Lebedev (1969) have shown that the peak-to-peak experimental line width is given by

$$\delta H^{PP} = \delta H_L^{PP}/2 + [(\delta H_G^{PP})^2 + (\delta H_L^{PP})^2/4]^{1/2} \quad (8)$$

where δH_L^{PP} and δH_G^{PP} are the peak-to-peak first-derivative Lorentzian and Gaussian line widths, respectively. Making the approximation that the inhomogeneous broadening is considerably greater than the Lorentzian broadening ($\delta H_G^{PP} \gg \delta H_L^{PP}$) and substituting from eq 7 for the Lorentzian line width, the peak-to-peak experimental line width is given by

$$\delta H^{PP} = (\hbar/\sqrt{3}g\beta)\tau_f^{-1} + \delta H_G^{PP} \quad (9)$$

where g is the nitroxide g value and other symbols have their usual meaning.

The data obtained from simulations for the low-field ($m_I = +1$) and high-field ($m_I = -1$) lines of the fluid component are plotted against the corresponding exchange rate constant in Figure 2. Data for the central hyperfine line are not included because this is obscured by a strong overlap with the motionally restricted component. As seen from the figure, both line widths have a linear dependence on the on-rate constant, τ_f^{-1}, predicted by eq 9, but with rather different gradients: 2.9×10^4 and 2.0×10^4 G·s for the low-field and high-field lines, respectively. The gradient predicted from eq 9 is 3.3×10^4 G·s, in reasonable agreement with the value from the simulations for the low-field line, which best approximates a single first-derivative line shape. The high-field line still contains contributions from residual anisotropy (cf. Figure 1) and therefore conforms less well to the conditions for applicability of eq 9 and has a lower sensitivity to exchange.

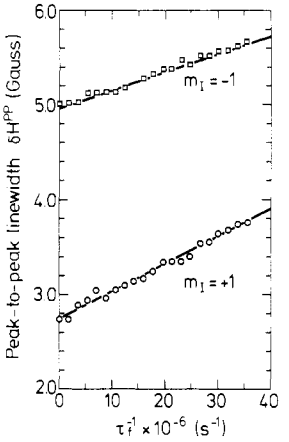

FIGURE 2: Calibration of the lifetime line-broadening effect of the bulk-to-boundary exchange on the line width of the fluid lipid component. (○) Low-field ($m_I = +1$) line width and (□) high-field ($m_I = -1$) line width, as a function of exchange rate, τ_f^{-1}.

The agreement of eq 9 with the simulations for the low-field line indicates that the spectra are in the slow-exchange regime over the range of on-rate constants $\tau_f^{-1} = 0$ to 4×10^7 s^{-1}, which is that appropriate to the experimental spectra in the present study. The analysis further demonstrates that the low-field fluid component is the region most sensitive to exchange and therefore deserves closest attention in the simulations. Equation 9 also provides a quick method for estimating exchange rates from the line width of the low-field fluid component, although total simulation is to be preferred since, as indicated below, optimization procedures can be used to fit the entire simulated line shape to the experimental spectrum.

Results

The first step in the simulation of the exchange-coupled ESR spectra from the lipid/protein recombinants is to simulate the spectra of the individual components in the absence of exchange. This is illustrated in Figure 3 for the spectra of dimyristoylphosphatidylcholine alone (Figure 3b) and for the delipidated protein (Figure 3c). A simplified model is employed for the single components which involves a single order parameter (which can be specified by the outer hyperfine splitting, A_{max}) and three independently variable Lorentzian line widths, $T_2^{-1}(m_I)$. The best fit parameters for the single-component spectra are given in the supplementary material (see paragraph at end of paper regarding supplementary material). Axial g tensors ($g_\parallel$, $g_\perp$) and hyperfine tensors ($A_\parallel$, $A_\perp$) have been assumed.

Comparison of an experimental spectrum for a proteolipid protein/dimyristoylphosphatidylcholine recombinant with simulated two-component spectra for various exchange rates, τ_b^{-1}, is given in Figure 4. For each value of the exchange rate the relative proportions of the two components f have been held at the optimum value of 0.71. It should be noted that the pure lipid and "protein-alone" components are taken to be those recorded at exactly the same temperature (30 °C) as that of the recombinant. From Figure 4 it can be seen that a reasonably good fit to the experimental spectrum can be obtained with an exchange rate in the region of 5×10^6 s^{-1}. The fit is not perfect in the high-field region of the fluid component, possibly due to some static perturbation by the protein causing an increase in the anisotropy of motion of the fluid lipids. However, it should be remembered that the simplified model that had to be used to simulate the individual components does not take adequate account of motional anisotropy. With these

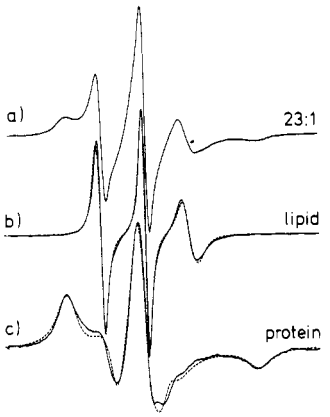

FIGURE 3: Simulation of single-component spectra with the 14-PASL phosphatidic acid spin-label: (a) myelin proteolipid apoprotein/DMPC recombinant of lipid/protein mole ratio 23:1; (b) DMPC alone; (c) myelin proteolipid apoprotein alone. Each spectrum was recorded at 30 °C. Full lines are experimental spectra, and broken lines are simulated spectra.

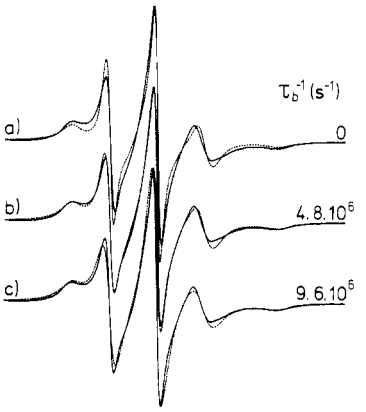

FIGURE 4: Comparison of experimental and simulated ESR spectra for various values of the exchange rate, τ_b^{-1}. Full lines in all three traces: spectrum of 14-PASL phosphatidic acid spin-label in a myelin proteolipid apoprotein/DMPC complex of lipid/protein ratio 23:1 mol/mol at 30 °C. Broken lines: simulated spectra with $f = 0.71$ and (a) $\tau_b^{-1} = 0$ (rms fitting error = 4.9%), (b) $\tau_b^{-1} = 4.8 \times 10^6\ s^{-1}$ (rms fitting error = 0.8%), and (c) $\tau_b^{-1} = 9.6 \times 10^6\ s^{-1}$ (rms fitting error = 2.8%).

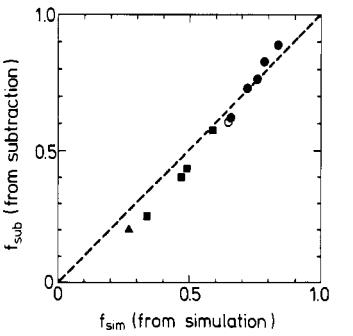

FIGURE 5: Comparison of the fractions of motionally restricted lipid in myelin proteolipid/DMPC recombinants obtained by spectral subtraction, f_{sub}, and by spectral simulation including exchange, f_{sim}. Spectra from recombinants at various lipid/protein ratios were recorded at 30 °C: (●) 14-PASL phosphatidic acid spin-label; (■) 14-PCSL phosphatidylcholine spin-label; (○) 14-PSSL phosphatidylserine spin-label; (▲) 14-PESL phosphatidylethanolamine spin-label.

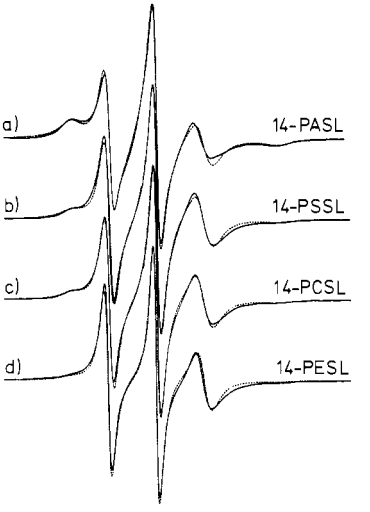

FIGURE 6: Comparison of experimental (full line) and simulated (broken line) spectra of a myelin proteolipid apoprotein/DMPC complex of lipid/protein ratio 23:1 at 30 °C with different phospholipid spin-labels: (a) phosphatidic acid, 14-PASL; (b) phosphatidylserine, 14-PSSL; (c) phosphatidylcholine, 14-PCSL; (d) phosphatidylethanolamine, 14-PESL.

reservations in mind, the agreement with the experimental spectrum is rather good in the low-field and central regions of the fluid component, that is, in those regions that might expect to be most sensitive to exchange.

In order to establish some objective assessment of the goodness of fit, a search routine (steepest descents) has been used to minimize the sums of squares of the differences between simulated and experimental spectra. To give some idea of the reliability and sensitivity of the method, root mean square (rms) error contour plots, as a function of the parameters, f and τ_b^{-1}, to be optimized, were constructed. Typically rms errors obtained in this way for the best fit are ~0.8%. For the case corresponding to Figure 4, there is an uncertainty of ~3% in f and of ~20% in τ_b^{-1}. Therefore, it appears that values for the fraction of motionally restricted lipid, f, might be determined from the simulations to a reasonably high degree of accuracy. It is of considerable technical interest to compare these values with those obtained by conventional spectral subtraction. In the latter case any effects of exchange are allowed for empirically by choosing the individual spectral components recorded at temperatures slightly different from that for the composite recombinant spectrum [see, e.g., Brophy et al. (1984) and Marsh (1982)]. The values of f deduced from the two different methods, for PLP/DMPC recombinants of various lipid/protein ratios and with different spin-labels, are plotted against each other in Figure 5. It is seen that there is quite good agreement between the results for the two methods, over the entire range of experimental values for the fraction of motionally restricted lipid. The most significant deviations occur at the lower values of f, but even then are maximally 30%. It thus appears that the subtraction strategy of empirically matching the two spectral components is reasonably effective in allowing for the effects of exchange.

Representative simulations for the phosphatidic acid, phosphatidylserine, phosphatidylcholine, and phosphatidylethanolamine spin-labels in PLP/DMPC recombinants of a fixed lipid/protein ratio are given in Figure 6. These simulations are for a single temperature and were all performed with the same single-component spectra; only the relative proportions and the exchange rates were varied. It is seen from Figure 6 that a consistent fit for all the spectra may be obtained in this way. The best fit values for the motionally

Table I: Best Fit Parameters from Two-Component Exchange Simulations of the ESR Spectra from Myelin Proteolipid Apoprotein/Dimyristoylphosphatidylcholine Recombinants at 30 °C

spin probe	lipid/protein (mol/mol)	f		τ_b^{-1} (s^{-1})
14-PASL	27	0.66		5.3×10^6
	23	0.71		4.8×10^6
	22	0.76		4.5×10^6
	17	0.79		4.9×10^6
	12	0.84		3.4×10^6
			mean:	4.6×10^6
14-PCSL	34	0.34		1.9×10^7
	29	0.47		1.6×10^7
	23	0.49		1.4×10^7
	10	0.49		1.5×10^7
	12	0.59		1.4×10^7
			mean:	1.6×10^7
14-PSSL	23	0.52		1.1×10^7
14-PESL	23	0.36		2.2×10^7

restricted fraction, f, and the exchange off-rate constant, τ_b^{-1}, established with the criteria described above, are given in Table I, which also contains data for recombinants of various lipid/protein ratios. It is found that, whereas the off-rate constant is essentially independent of the lipid/protein ratio for a given spin-label, the lipid selectivity is reflected by the different off-rate constants for the different spin-labeled lipids.

Fits have also been made to the temperature dependence of the spectra, using simulations from the two-component exchange model. The fraction of motionally restricted lipid decreases somewhat with increasing temperature, and the exchange rate increases with increasing temperature, as is to be expected. An Arrhenius plot of the temperature dependence of the off-rate constant for the 14-PASL spin-label in a PLP/DMPC recombinant is given in Figure 7. The temperature dependence is biphasic, conforming well to an Arrhenius law in the fluid phase of DMPC, with an activation energy of 24 kJ·mol^{-1} (5.7 kcal·mol^{-1}). In the phase-transition region the temperature dependence is much steeper, with an effective activation energy in the region of 55 kJ·mol^{-1}.

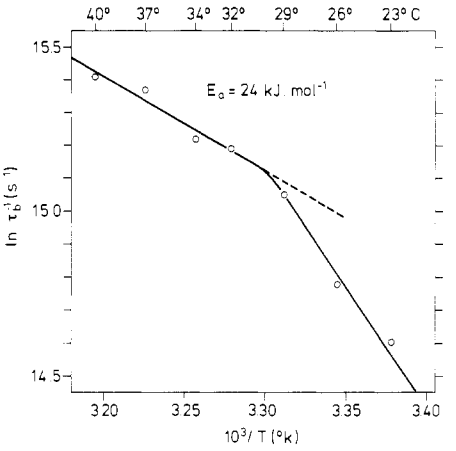

FIGURE 7: Arrhenius plot of the exchange lifetime τ_b^{-1} vs $1/T$ obtained from simulation of the temperature dependence of the spectra from a myelin proteolipid apoprotein/DMPC complex of lipid/protein ratio 23:1 mol/mol labeled with the 14-PASL phosphatidic acid spin-label.

DISCUSSION

The satisfactory fit between the experimental spectra for PLP/DMPC recombinants and the simulations for slow exchange further supports the two-component model used previously to interpret the spin-label ESR spectra for both this and other lipid–protein systems (Brophy et al., 1984; Marsh, 1985). In addition, the results of Figure 5 also validate the subtraction strategy normally used for determining the relative proportions of the fluid and motionally restricted components in the composite spectra. More importantly, the lipid exchange rate may be determined with a reasonable degree of accuracy, if objective criteria are used to assess the quality of fit between experimental and simulated spectra.

The degree of discrimination is relatively high. For example, the exchange rate used for the simulation in Figure 4c is that which when corrected for the selectivity gives the best fit to the spectrum of the phosphatidylcholine spin-label. This clearly gives a fit to the experimental spectrum of the phosphatidic acid spin-label that is inferior to the optimum simulation which is given in Figure 4b. It is therefore possible to make significant comparisons between the lipid-exchange dynamics at different temperatures and lipid/protein ratios, and for different spin-labeled lipids.

The off-rate constant for exchange is found to be approximately independent of lipid/protein ratio for both spin-labeled phosphatidic acid and spin-labeled phosphatidylcholine (see Table I). This is to be expected, provided that the number of second-shell lipids available for exchange is not limiting and that there is rapid equilibration by lateral diffusion within the pool of fluid, exchangeable lipids. In contrast, lipid selectivity is expected to affect the off-rate for exchange, since a longer residence time in the first lipid shell will correspond to a stronger selectivity. This is found to be the case for the results of Table I. The lipids with the lower off-rate constants are just those for which a specificity for the myelin proteolipid protein has previously been demonstrated (Brophy et al., 1984).

Quantitatively, the dependence on selectivity can be understood in terms of the equation for equilibrium association between lipid and protein (Brotherus et al., 1981; Brophy et al., 1984):

$$(n_f^*/n_b^*) = (1 - f)/f = n_t/(N_1 K_r^{av}) - 1/K_r^{av} \quad (10)$$

where (n_f^*/n_b^*) is the ratio of the number of fluid to motionally restricted lipids, n_t is the total number of lipids per protein in the recombinant, N_1 is the number of first-shell lipid sites per protein, and K_r^{av} is the average relative association constant for all sites. The association constant K_r^{av} is defined relative to the host background lipid (in this case DMPC), with which the spin-labeled lipid is competing for sites on the protein. Substituting from eq 3, the ratio of exchange rate constants therefore becomes

$$\tau_b^{-1}/\tau_f^{-1} = n_t/(N_1 K_r^{av}) - 1/K_r^{av} \quad (11)$$

If it is assumed that, for a given lipid/protein ratio, the on-rate constant, τ_f^{-1}, is the same for all lipids, i.e., that it is diffusion controlled, then for different lipid spin-labels, say L and PC, the ratio of the off-rate constants is

$$\tau_b^{-1}(PC)/\tau_b^{-1}(L) = K_r^{av}(L)/K_r^{av}(PC) \quad (12)$$

From Table I, the ratios of the rate constants are $\tau_b^{-1}(PC)/\tau_b^{-1}(PA) = 3.5$, $\tau_b^{-1}(PC)/\tau_b^{-1}(PS) = 1.4$, and $\tau_b^{-1}(PC)/\tau_b^{-1}(PE) = 0.7$, as compared with values of $K_r^{av}(PA)/K_r^{av}(PC) = 3.0$, $K_r^{av}(PS)/K_r^{av}(PC) = 1.2$, and $K_r^{av}(PE)/K_r^{av}(PC) = 0.6$, for the ratios of the relative equilibrium association constants deduced from the values of $(1 - f)/f$ in Table I [see also Brophy et al. (1984)].

Thus, the experimental values for the exchange rate con-

stants display the expected dependence on both lipid/protein ratio and lipid selectivity. This gives confidence in the sensitivity and reliability of the simulations and strongly suggests that the main source of spectral broadening comes from exchange rather than more direct lipid–protein interactions. The measured off-rate constants for phosphatidylcholine are of the same order of magnitude, although significantly slower, than the exchange rates for lateral diffusion in fluid lipid bilayers. This is consistent with the results of ^2H NMR experiments on the same system (Meier et al., 1987), which indicate that there is fast exchange between all lipid components on the milli- to microsecond time scale and therefore that there is no long-lived association of phosphatidylcholine at the intramembranous surface of the reconstituted myelin proteolipid protein. The temperature dependence of the off-rate is also in agreement with this conclusion, since this is characterized by an activation energy of ca. 24 kJ·mol^{-1} for phosphatidic acid at temperatures above the phase transition of DMPC. The latter value lies within the range of activation energies found for lateral diffusion in fluid-phase lipid bilayers [see, e.g., Marsh (1987)], further indicating that a strong activation barrier is not involved in the interaction of the lipids with the protein.

It is also of interest to compare with similar measurements from other systems. The off-rate constant for phosphatidylcholine in rhodopsin/DMPC recombinants is 1.6×10^7 s^{-1} (Ryba et al., 1987), which is the same as is given for the PLP/DMPC recombinants in Table I. An off-rate constant of 2×10^7 s^{-1} at 37 °C has also been determined for phosphatidylcholine interacting with the Ca^{2+}-ATPase from sarcoplasmic reticulum (East et al., 1985), although this may not be strictly comparable with the present work, since a dependence of the off-rate on lipid/protein ratio was reported for the Ca^{2+}-ATPase. In contrast to PLP, little lipid selectivity is found for the latter two proteins [see, e.g., Marsh (1985)].

The lipid exchange rate due to lateral diffusion in dimyristoylphosphatidylcholine bilayers at 30 °C has been determined to be $\tau_{dif}^{-1} = 4D_T/\langle x^2 \rangle \sim 3.7 \times 10^7$ s^{-1} by photobleaching (Vaz et al., 1985) and 7.5×10^7 s^{-1} for spin-labeled phosphatidylcholine by ESR spectroscopy (Sachse et al., 1987). These rates are appareciably faster than the one-to-one lipid exchange on and off the protein, which is characterized by the values of τ_b^{-1} for phosphatidylcholine in Table I. The reason for this could be partly geometrical, in that the lipid–protein interface forces the exchange to be essentially unidirectional, as well as being partly energetic. Thermodynamically the effect can be characterized by an effective association constant: $K_{eff}^{av} = \tau_{dif}^{-1}/\tau_b^{-1}$, where the effective on-rate constant, τ_{dif}^{-1}, is taken to be diffusion controlled. Experiments on the collision rates between diffusible ^{14}N-labeled lipids and ^{15}N-labeled chains covalently linked to the protein have shown the latter to be the case for rhodopsin–lipid recombinants (Davoust et al., 1983). (Note that the on-rate constant, τ_f^{-1}, in eq 3 merely reflects detailed balance for the one-to-one exchange at the lipid–protein interface and is therefore not relevant to the energetics of the interaction.) The values for the effective association constant for phosphatidylcholine with the myelin proteolipid protein are therefore $K_{eff}^{av} \sim 2$–5, corresponding to a free energy of interaction of $\Delta G \sim -1.7$ to -4.1 kJ·mol^{-1}, indicating that the lipid–protein interaction is not very strongly favored energetically over the lipid–lipid interactions.

In summary, therefore, the measured exchange rates reflect very directly the thermodynamics of the lipid–protein interaction, as characterized previously by spectral subtraction (Brophy et al., 1984). This both gives support for the two-component methods of spectral analysis employed previously and also indicates that the two-site exchange simulations are capable of giving reasonably accurate estimates of the exchange frequency. The free energy associated with the lipid–protein interaction may be up to -4 kJ·mol^{-1} greater than that for the lipid–lipid interactions, and that associated with the lipid selectivity of the lipid–protein interaction is also of the same order of magnitude. The major contribution to the energetics of the lipid–protein interaction is therefore the same as that for the lipid–lipid interaction, namely, the hydrophobic effect [see, e.g., Cevc and Marsh (1987)]. This can be estimated from the critical micelle concentration for DMPC to be on the order of -57 kJ·mol^{-1} (Marsh & King, 1986). The result is that the exchange rate at the lipid–protein interface is relatively rapid for nearly all lipids and provides the necessary dynamic coupling for integrating the relatively rigid protein backbone into the fluid lipid environment.

ACKNOWLEDGMENTS

We thank S. Chatterjee for her technical assistance in the protein preparation.

SUPPLEMENTARY MATERIAL AVAILABLE

Table containing simulation parameters [hyperfine tensors $A_\parallel$ and $A_\perp$; g tensors $g_\parallel$ and $g_\perp$; maximum hyperfine splitting A_{max}; line widths $T_2^{-1}(m_I)$] of the single-component spectra, for both pure lipid and protein-alone samples at various temperatures over the range 1–40 °C (1 page). Ordering information is given on any current masthead page.

Registry No. DMPC, 18194-24-6.

REFERENCES

Brophy, P. J. (1977) *FEBS Lett. 84*, 92–95.
Brophy, P. J., Horváth, L. I., & Marsh, D. (1984) *Biochemistry 23*, 860–865.
Brotherus, J. R., Griffith, O. H., Brotherus, M. O., Jost, P. C., Silvius, J. R., & Hokin, L. E. (1981) *Biochemistry 20*, 5261–5267.
Cevc, G., & Marsh, D. (1987) *Phospholipid Bilayers. Physical Principles and Models*, 442 pp, Wiley-Interscience, New York.
Davoust, J., & Devaux, P. F. (1982) *J. Magn. Reson. 48*, 475–494.
Davoust, J., Seigneuret, M., Hervé, P., & Devaux, P. F. (1983) *Biochemistry 22*, 3146–3151.
East, J. M., Melville, D., & Lee, A. G. (1985) *Biochemistry 24*, 2615–2623.
Eibl, H., & Lands, W. E. M. (1969) *Anal. Biochem. 30*, 51–57.
Jost, P. C., Griffith, O. H., Capaldi, R. A., & Vanderkooi, G. (1973) *Proc. Natl. Acad. Sci. U.S.A. 70*, 4756–4763.
Kang, S. Y., Gutowsky, H. S., Hsung, J. C., Jacobs, R., King, T. E., Rice, D., & Oldfield, E. (1979) *Biochemistry 18*, 3257–3267.
Knowles, P. F., Watts, A., & Marsh, D. (1979) *Biochemistry 18*, 4480–4487.
Laemmli, U. K. (1970) *Nature (London) 227*, 680–685.
Lowry, O. H., Rosebrough, N. J., Farr, L., & Randall, R. J. (1951) *J. Biol. Chem. 193*, 265–275.
Marsh, D. (1982) *Tech. Life Sci.: Biochem. B4/II*, B426/1–B426/44.

Marsh, D. (1985) in *Progress in Protein-Lipid Interactions* (Watts, A., & De Pont, J. J. H. H. M., Eds.) Vol. 1, pp 143-172, Elsevier, Amsterdam.
Marsh, D. (1987) *Handbook of Lipid Bilayers*, CRC Press, Boca Raton, FL.
Marsh, D., & Watts, A. (1982) in *Lipid-Protein Interactions* (Jost, P. C., & Griffith, O. H., Eds.) Vol. 2, pp 53-156, Wiley-Interscience, New York.
Marsh, D., & King, M. D. (1986) *Chem. Phys. Lipids 42*, 271-277.
McConnell, H. M. (1958) *J. Chem. Phys. 28*, 430-431.
Meier, P., Sachse, J.-H., Brophy, P. J., Marsh, D., & Kothe, G. (1987) *Proc. Natl. Acad. Sci. U.S.A. 84*, 3704-3708.
Ryba, N. J., Horvâth, L. I., Watts, A., & Marsh, D. (1987) *Biochemistry 26*, 3234-3240.
Sachse, J.-H., King, M. D., & Marsh, D. (1987) *J. Magn. Reson. 71*, 385-404.
Seelig, J., Seelig, A., & Tamm, L. (1982) in *Lipid-Protein Interactions* (Jost, P. C., & Griffith, O. H., Eds.) Vol. 2, pp 127-148, Wiley-Interscience, New York.
Vaz, W. L. C., Clegg, R. M., & Hallmann, D. (1985) *Biochemistry 24*, 781-786.

Lipid Composition of PC12 Pheochromocytoma Cells: Characterization of Globoside as a Major Neutral Glycolipid†

Toshio Ariga,‡ Lawrence J. Macala,‡ Megumi Saito,‡ Renee K. Margolis,§ Lloyd A. Greene,∥ Richard U. Margolis,∥ and Robert K. Yu*,‡

Department of Neurology, Yale University School of Medicine, New Haven, Connecticut 06510, Department of Pharmacology, State University of New York Health Science Center at Brooklyn, Brooklyn, New York 11203, and Department of Pharmacology, New York University Medical Center, New York, New York 10016

Received June 9, 1987; Revised Manuscript Received August 18, 1987

ABSTRACT: We have studied the lipid composition of PC12 pheochromocytoma cells cultured in the presence and absence of nerve growth factor (NGF). Neutral and acidic lipid fractions were isolated by column chromatography on DEAE-Sephadex and analyzed by high-performance thin-layer chromatography (HPTLC). The total lipid concentration was approximately 220 μg/mg of protein, and the concentration of neutral glycolipids was 1.6–1.8 μg/mg of protein for both NGF-treated and untreated cells. The neutral glycolipid fraction contained a major component, which accounted for approximately 80% of the total and which was characterized as globoside on the basis of HPTLC mobility, carbohydrate analysis, fast atom bombardment mass spectrometry, and mild acid hydrolysis. The major fatty acids of globoside were C16:0 (10%), C18:0 (16%), C22:0 (23%), C24:1 (17%), and C24:0 (24%). C18 sphingenine accounted for almost all of the long-chain bases. The other neutral glycolipids were tentatively identified as glucosylceramide (15%), lactosylceramide (4%), and globotriosylceramide (4.5%). The concentration of ganglioside sialic acid was approximately 0.34 and 0.18 μg/mg of protein for cells grown in the presence and absence of NGF, respectively. Although there was an increase in ganglioside concentration in NGF-treated cells, NGF did not produce any differential effects on the relative proportions of the individual gangliosides. Several of the gangliosides appear to contain fucose, and one of these was tentatively identified as fucosyl-GM_1. Brain-type gangliosides of the ganglio series were also detected by an HPTLC–immunostaining method. However, the fatty acid and long chain base compositions of PC12 cell gangliosides (and their TLC mobility) differ from those of brain gangliosides. The major lipids of PC12 cells, which were not significantly affected by NGF treatment, were phosphatidylcholine (40%), phosphatidylethanolamine (22%), and cholesterol (13%).

The PC12 cells, a clonal line of rat adrenal medullary pheochromocytoma cells, display many properties associated with normal adrenal chromaffin cells and undergo striking morphological and physiological changes in response to nerve growth factor (NGF),[1] which converts them into a sympathetic neuron-like phenotype [for a review, see Greene and Tischler (1982)]. Glycosphingolipids have been shown to be located almost exclusively in the outer leaflet of plasma membranes and have been implicated in many cell surface phenomena (Hakomori, 1981). In spite of the utility of PC12 cells for the study of various types of cell surface events, little is known concerning their complex glycosphingolipid composition. It was previously reported that NGF treatment produces an almost 3-fold increase in the incorporation of labeled gluco-

† This work was supported by grants from the National Institutes of Health (NS-09348, NS-11853, NS-13876, NS-16036, and NS-23102).
* Address correspondence to this author.
‡ Yale University School of Medicine.
§ State University of New York Health Science Center at Brooklyn.
∥ New York University Medical Center.

[1] Abbreviations: Cer, ceramide (*N*-acylsphingoid); GlcCer, Glcβ1-1Cer; LacCer, Galβ1-4Glcβ1-1Cer; Gg_3 (asialo-G_{M2}), GalNAcβ1-4Galβ1-4Glcβ1-1Cer; Gg_4 (asialo-G_{M1}), Galβ1-3GalNAcβ1-4Galβ1-4Glcβ1-1Cer; Gb_3, Galα1-4Galβ1-4Glcβ1-1Cer; Gb_4 (globoside), GalNAcβ1-3Galα1-4Galβ1-4Glcβ1-1Cer; Gb_5, GalNAcα1-3GalNAcβ1-3Galα1-4Galβ1-4Glcβ1-1Cer; NeuAc, *N*-acetylneuraminic acid; G_{M3}, NeuAcα2-3Galβ1-4Glcβ1-1Cer; G_{M2}, GalNAcβ1-4Gal(3-2αNeuAc)β1-4Glcβ1-1Cer; G_{M1}, Galβ1-3GalNAcβ1-4Gal(3-2αNeuAc)β1-4Glcβ1-1Cer; G_{D1a}, NeuAcα2-3Galβ1-3GalNAcβ1-4Gal(3-2αNeuAc)β1-4Glcβ1-1Cer; G_{D1b}, Galβ1-3GalNAcβ1-4Gal(3-2αNeuAc8-2αNeuAc)β1-4Glcβ1-1Cer; G_{D3}, NeuAcα2-8NeuAcα2-3Galβ1-4Glcβ1-1Cer; G_{D2}, GalNAcβ1-4Gal(3-2αNeuAc8-2αNeuAc)β1-4Glcβ1-1Cer; fucosyl-G_{M1} (or G_{M1}-Fuc), Fucα1-2Galβ1-3GalNAcβ1-4Gal(3-2αNeuAc)β1-4Glcβ1-1Cer; G_{T1b}, NeuAcα2-3Galβ1-3GalNAcβ1-4Gal(3-2αNeuAc8-2αNeuAc)β1-4Glcβ1-1Cer; G_{Q1b}, NeuAcα2-8NeuAcα2-3Galβ1-3GalNAcβ1-4Gal(3-2αNeuAc8-2αNeuAc)β1-4Glcβ1-1Cer; NGF, nerve growth factor; HPTLC, high-performance thin-layer chromatography; GLC, gas–liquid chromatography.

0006-2960/88/0427-0052$01.50/0